

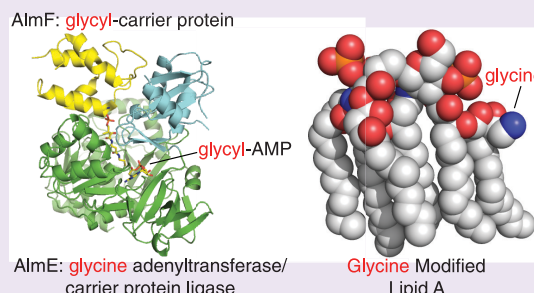
# Antimicrobial Peptide Resistance of *Vibrio cholerae* Results from an LPS Modification Pathway Related to Nonribosomal Peptide Synthetases

Jeremy C. Henderson,<sup>†,||</sup> Christopher D. Fage,<sup>†,||</sup> Joe R. Cannon,<sup>‡</sup> Jennifer S. Brodbelt,<sup>‡</sup> Adrian T. Keatinge-Clay,<sup>\*,†,§</sup> and M. Stephen Trent<sup>\*,†,§</sup>

<sup>†</sup>Department of Molecular Biosciences, <sup>‡</sup>Department of Chemistry, <sup>§</sup>Institute of Cellular and Molecular Biology, The University of Texas at Austin, Austin, Texas 78712, United States

## S Supporting Information

**ABSTRACT:** The current pandemic El Tor biotype of O1 *Vibrio cholerae* is resistant to polymyxins, whereas the previous pandemic strain of the classical biotype is polymyxin sensitive. The *almEFG* operon found in El Tor *V. cholerae* confers >100-fold resistance to polymyxins through the glycation of lipopolysaccharide. Here, we present the mechanistic determination of initial steps in the AlmEFG pathway. We verify that AlmF is an aminoacyl carrier protein and identify AlmE as the enzyme required to activate AlmF as a functional carrier protein. A combination of structural information and activity assays was used to identify a pair of active site residues that are important for mediating AlmE glycine specificity. Overall, the structure of AlmE in complex with its glycyladenylate intermediate reveals that AlmE is related to Gram-positive D-alanine/D-alanyl carrier protein ligase, while the trio of proteins in the AlmEFG system forms a chemical pathway that resembles the division of labor in nonribosomal peptide synthetases.



Clinical use of polymyxins has emerged as the antibacterial strategy of last resort for infections with multidrug resistant Gram-negative bacteria such as *Acinetobacter baumanii*, *Pseudomonas aeruginosa*, *Klebsiella* spp., and *E. coli* spp.<sup>1–3</sup> Polymyxins are cationic antimicrobial peptides (CAMPs) comprising a cationic/hydrophobic cyclic decapeptide linked to a fatty acyl chain. Like host defensins, CAMPs disrupt the Gram-negative cell envelope by associating with the anionic lipid A membrane anchor of the major cell-surface molecule lipopolysaccharide (LPS) as well as acidic glycerophospholipids.<sup>3</sup> Detergent-like aggregates of membrane-bound polymyxins form pores in the associated membrane, disrupting vital bacterial processes.<sup>3</sup> Accumulating evidence suggests that many bacteria have evolved elegant resistance strategies toward polymyxins and related families of CAMPs.<sup>3,4</sup> For this reason, a comprehensive understanding of the molecular basis for resistance to CAMPs is paramount in designing new, or modifying current, antibiotics and in developing improved clinical regimens with existing drugs.

In general, to evade CAMP-mediated killing, Gram-negative and Gram-positive bacteria have evolved similar strategies to neutralize the net negative charge of major cell-surface molecules. Phosphatidylglycerols aminoacylated with L-lysine, L-alanine, or D-alanine were recently discovered and confer resistance toward CAMPs in a few species of both Gram-type bacteria (e.g., *Staphylococcus aureus* and *P. aeruginosa*).<sup>5</sup> Gram-positive bacteria commonly neutralize their cell walls by transferring D-alanine to surface teichoic acids, the long poly-

phosphoribitol or poly phosphoglycerol chains linked to the glycerophospholipids or N-acetylmuramic acid groups of peptidoglycan;<sup>6</sup> Gram-negative bacteria do so by transferring phosphoethanolamine or aminoarabinose to phosphate groups on the lipid A domain of LPS.<sup>7,8</sup> Unexpectedly, we observed aminoacyl esterification of glycine or diglycine to lipid A of the Gram-negative pathogen *Vibrio cholerae*.<sup>9</sup> Lipid A glycation is a unique Gram-negative strategy necessary for resistance to CAMPs, which resembles the Gram-positive method of modifying teichoic acids with D-alanine.

Unlike the O1 classical biotype of *V. cholerae*, which caused the first six cholera pandemics, the O1 El Tor biotype responsible for the most recent pandemic is resistant to polymyxin B.<sup>10</sup> El Tor strains are responsible for the majority of 3–5 million cases and 100,000–120,000 deaths associated with *V. cholerae* infection every year (World Health Organization). AlmE (Vc1579), AlmF (Vc1578), and AlmG (Vc1577) were identified by our laboratory as three gene products required for polymyxin B resistance in El Tor biotype *V. cholerae* O1.<sup>9</sup> Together, these enzymes orchestrate the modification of *V. cholerae* lipid A with glycine or diglycine (Figure 1). According to our proposed model, AlmE activates glycine through adenylation and then transfers it to the 4'-phosphopantetheine

Received: June 3, 2014

Accepted: July 28, 2014

Published: July 28, 2014



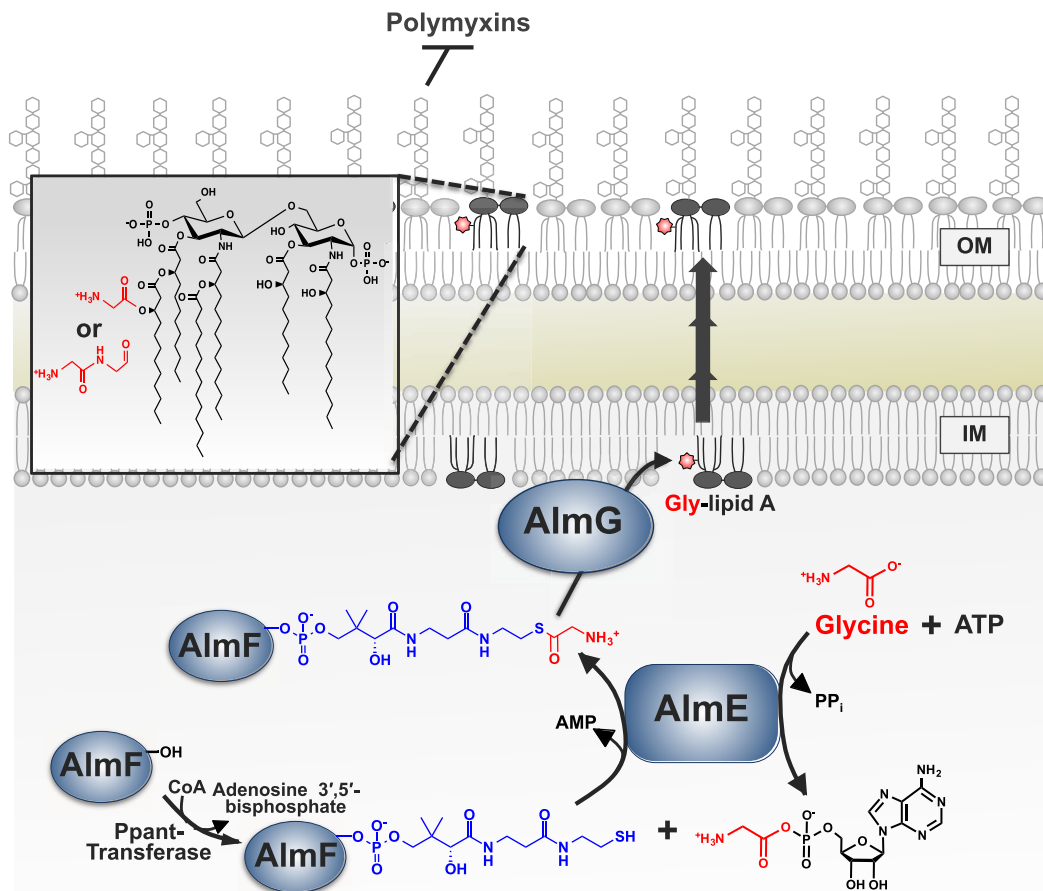


**Figure 1.** Proposed model for the lipid A glycation pathway in *V. cholerae*. AlmE (Vc1579) generates glycyl-AMP and pyrophosphate from glycine and ATP. Glycine is then ligated onto carrier protein holo-AlmF (Vc1578) with concomitant release of AMP. Holo-AlmF is generated after the 4'-phosphopantetheinyl (Ppant) moiety of coenzyme A is transferred onto apo-AlmF by the phosphopantetheinyltransferase. At the inner membrane, glycyl-AlmF serves as the aminoacyl donor to AlmG (Vc1577), which esterifies glycine onto the secondary hydroxylauryl acyl chain of *V. cholerae* hexa-acylated lipid A. Glycine-modified lipid A is then transported to the bacterial surface to provide resistance against antimicrobial peptides such as polymyxin.

group of the carrier protein AlmF. AlmG then transfers the glycine substrate from the carrier AlmF to the lipid A anchor. A unique hydroxylauryl chain observed in the lipid A species from El Tor biotype *V. cholerae* serves as the site of glycine addition,<sup>11</sup> making AlmEFG the only known lipid A charge remodeling system that does not involve direct transfer to the 1- or 4'-phosphate groups of lipid A. Notably, the classical biotype *V. cholerae*, which does not attach glycine to lipid A and is thus polymyxin-sensitive, encodes a truncated AlmF lacking the predicted phosphopantetheinylation site necessary for its proposed carrier protein functionality.<sup>9</sup>

A pair of studies has revealed that the AlmEFG pathway is important during early stages of infection and initial host colonization by *V. cholerae*.<sup>12,13</sup> In *V. cholerae* isolated from infant mouse small intestine, the mRNA transcript of the *almEFG* operon is upregulated >10-fold.<sup>13</sup> Moreover, microarray-based comparative gene expression analysis showed a 3.2-fold increase (*p*-value  $1.6 \times 10^{-6}$ ) in AlmE levels between early- and late-stage infections of humans by *V. cholerae*.<sup>12</sup> In that report, AlmE was 1 of 42 statistically significant, differentially regulated genes to be identified. As evidence accumulates to demonstrate the importance of the AlmEFG system during infection, detailed mechanistic studies of AlmEFG have the potential to inform further research on therapeutic drugs and vaccines targeting *V. cholerae* infections.

Here, we present the first detailed molecular mechanism of lipid A glycation in *V. cholerae*. Mass spectrometry data verify that AlmF is a *bona fide* glycol carrier protein and that moreover AlmE can transfer glycine to its 4'-phosphopantetheine group. *In vitro* characterization of AlmE reveals that it also accepts D-alanine, albeit with reduced activity compared to that of glycine. To further investigate this surprising result, we determined the X-ray structure of AlmE in complex with a glycyl-adenylate intermediate at 2.26-Å resolution. Visualizing the active site of AlmE allowed us to rationally design a single-residue mutant capable of efficiently activating and transferring L-alanine to AlmF. However, *in vivo* evidence suggests that L-alanyl-AlmF is not a suitable substrate for AlmG, indicating that the AlmEFG pathway is strictly specific toward glycine. Selection of glycine as the group AlmEFG adds to lipid A likely balances deleterious effects larger amino acids would have on membrane packing while providing sufficient electropositive density to effectively resist CAMPs. Our findings provide molecular insight into a complex mechanism of CAMP resistance that incorporates preexisting chemistry, commonly found in nonribosomal peptide synthetases, into new biosynthetic pathways.

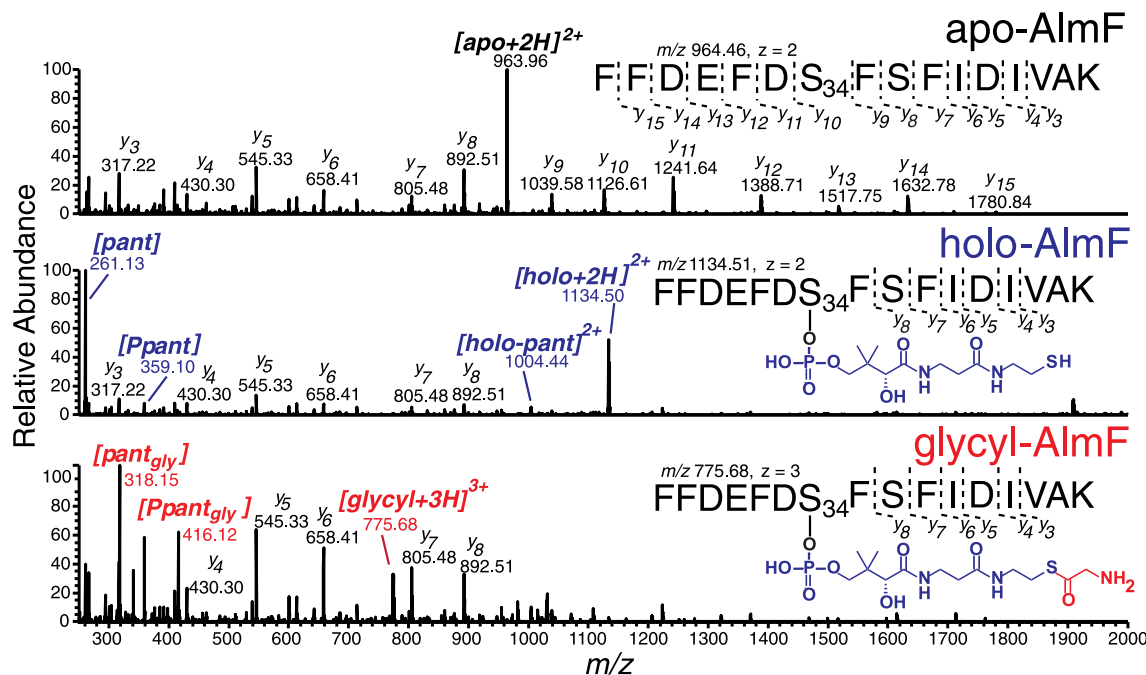


**Figure 2.** Ultraviolet photodissociation (UVPD)-MS/MS confirms AlmF phosphopantetheinylation by Vc2457 and subsequent glycation by AlmE when coexpressed in *E. coli*. Shown are MS<sup>2</sup> spectra resulting from 193 nm ultraviolet photodissociation of precursor ions corresponding to the trypsinized AlmF peptide FFDEFDS<sub>34</sub>FSFDIVAK: (top) doubly charged, unmodified (apo-AlmF; precursor *m/z* 964), (middle) doubly charged, Ppant-modified (holo-AlmF; precursor *m/z* 1134), and (bottom) triply charged, Ppant<sub>Gly</sub>-modified (glycyl-AlmF; precursor *m/z* 776). These samples were obtained from purified AlmF, AlmF coexpressed with Vc2457, or AlmF coexpressed with Vc2457 and AlmE, respectively. Ser34 is the Ppant modification site as the *y*-type ion series through Ser36 (*y*<sub>3</sub>–*y*<sub>8</sub>) is conserved for both Ppant-modified AlmF (middle) and Ppant<sub>Gly</sub>-modified AlmF (bottom). Cleavage on either side of the phospho group results in diagnostic Ppant modification ions in the low mass region: (middle) Pant (*m/z* 261) and Ppant (*m/z* 359) or (bottom) Pant<sub>Gly</sub> (*m/z* 318) and Ppant<sub>Gly</sub> (*m/z* 416). The most abundant fragment ions are labeled.

## RESULTS AND DISCUSSION

**AlmF Is Phosphopantetheinylated by Vc2457.** Homology-based structural data obtained from the Phyre2 server suggest that AlmF forms the same three-helix architecture observed in carrier proteins such as the Gram-positive D-alanyl carrier protein DltC, and harbors a conserved, nucleophilic serine residue at the N-terminal end of helix 2 (Figure S1, Supporting Information).<sup>14</sup> This serine residue is post-translationally modified with 4'-phosphopantetheine (Ppant), a thiol-containing prosthetic group that allows this class of proteins to shuttle substrate molecules as covalently attached thioesters.<sup>14</sup> A phosphopantetheinyltransferase appends the Ppant moiety from coenzyme A directly onto the carrier protein serine residue.<sup>15</sup> Bacteria encode at least two phosphopantetheinyl-transferases: one activates acyl carrier proteins (e.g., AcpS) necessary for primary metabolic reactions such as fatty acid biosynthesis, and another activates carrier proteins of the biosynthetic pathways producing secondary metabolites such as polyketide and nonribosomal peptide antibiotics.<sup>16</sup>

To determine if AlmF is a *bona fide* carrier protein, AlmF was coexpressed with either predicted phosphopantetheinyltransferase of *V. cholerae*, Vc2457 or Vc0780, and subsequently purified and examined for phosphopantetheinylation. To obtain quantities of AlmF suitable for analysis, proteins were overexpressed in *E. coli* BL21(DE3)pLysS using the pQLink system and purified by a two-step protocol, yielding >95% pure AlmF as evaluated by sodium dodecyl sulfate–polyacrylamide gel electrophoresis (SDS-PAGE) (Figure S2, Supporting Information). To assess phosphopantetheinylation, purified “Ppant-modified” (holo-) and “unmodified” (apo-) carrier proteins, were resolved on a nondenaturing, destabilizing

urea-PAGE gel.<sup>17–19</sup> AlmF coexpressed with Vc2457 displayed a migration shift consistent with Ppant-addition, compared to that with AlmF expressed alone or coexpressed with Vc0780 (Figure S3, Supporting Information). *E. coli* strains expressing AlmF alone yielded a band consistent with the predicted migration of holo-AlmF only after supplementing the media with millimolar concentrations of pantothenate (Figure S4, Supporting Information; <50% conversion), consistent with the nonspecific activity of *E. coli* AcpS on increased coenzyme A substrate pools (Figure S4, Supporting Information<sup>20</sup>). AlmF appears completely phosphopantetheinylated when coexpressed with *V. cholerae* AcpS (Vc2457) without pantothenate supplementation (Figures S3 and S4, Supporting Information).

Unequivocal determination of AlmF Ppant-modification was assessed by liquid chromatography–tandem mass spectrometry (LC-MS/MS) of trypsin-digested AlmF. Digests of unmodified (apo-AlmF; expressed alone) or Ppant-modified (holo-AlmF; coexpressed with Vc2457) AlmF were analyzed using the same purified AlmF material assessed by destabilizing urea-PAGE (Figures S3 and S4, Supporting Information). Three key peptides, each covering the first 41 amino acids of AlmF, were identified from LC-MS/MS analysis (Figure S5, Supporting Information). The AlmF peptide (FFDEFDSFSFDIVAK) containing the proposed site of modification, Ser34, eluted around 20 min in the apo-AlmF sample, whereas the same Ser34-containing peptide eluted 2 min later in the holo-AlmF sample, consistent with Ppant-addition (Figure S5, Supporting Information; *m/z* shift of 114 for the [M+3H]<sup>3+</sup> peptide). An increase in overall hydrophobicity is expected upon Ppant-addition, consistent with the delayed elution of the holo-AlmF peptide. The electrospray ionization mass spectrum of the holo-

AlmF Ser34-containing peptide showed a mass shift of ~340 Da relative to the apo-AlmF peptide, indicative of Ppant-modification (Figure 2). The sequence of the unmodified FFDEFDSFSFIDIVAK peptide ( $[M+2H^+]^{2+}$ ) was readily confirmed based on the presence of the  $y_3$  to  $y_{15}$  fragment ions (Figure 2, upper spectrum). MS/MS analysis of the peptide from the holo-AlmF sample resulted in a series of diagnostic  $y$  sequence ions as well as singly charged product ions corresponding to pantetheine (Pant,  $m/z$  261.1) and Ppant ( $m/z$  359.1) in the low-mass region (Figure 2, middle spectrum). Generation of Pant and Ppant product ions during MS/MS analysis of other Ppant-modified proteins has been previously reported.<sup>21</sup> It should be noted that while Ser36 of AlmE could serve as the Ppant-modification site, the observed  $y$ -type product ions containing Ser36 were matched to their expected, unmodified masses and thus did not exhibit the incorporation of Ppant (Figure 2, middle spectrum). Low-abundance  $y$ -type product ions (from  $y_{10}$  up to  $y_{15}$ ) that incorporated Ppant were also observed (Figure S6, Supporting Information), implicating Ser34 as the sole Ppant-modified site. Together with results from destabilizing urea-PAGE experiments, these findings convincingly support our structural homology-based prediction that AlmF is a Ppant-containing carrier protein.

Classical biotype O1 *V. cholerae* encodes a truncated version of AlmF that lacks the phosphopantetheinylation site required for carrier protein functionality. Thus, our biochemical determination that AlmF is a glycol carrier protein provides a rationale for why classical biotype O1 *V. cholerae* does not add glycine to lipid A and exhibits polymyxin sensitivity. Why classical strains appear to have lost carrier protein functionality and thus CAMP resistance is intriguing. Expression data reported from other laboratories show that *almEFG* is upregulated during early stages of *V. cholerae* infection in human volunteers and mouse infection models.<sup>12,13</sup> Improved CAMP resistance may have led to the emergence of El Tor over classical biotypes as the premier pandemic strain. However, the hypothesis that classical strains lost the ability to add glycine to the cell surface could mean that a modification of this type is detrimental to *V. cholerae* fitness under certain environmental conditions. Consistent with this hypothesis, our laboratory has recently discovered a two-component system responsible for regulating the AlmEFG system.

**AlmE Adds Glycine to the AlmF Carrier Protein.** To verify the role of AlmF as a glycol carrier protein, we engineered holo-AlmF-producing *E. coli* strains to express AlmE, the predicted carrier protein ligase. Unexpectedly, destabilizing urea-PAGE revealed no apparent shift in the migration of holo-AlmF when coexpressed with AlmE (Figure S4, Supporting Information). However, deeper analysis of this sample by the same LC-MS/MS protocols described above demonstrated that the Ppant-containing peptide was modified with glycine ( $m/z$  775.8,  $z = 3$ , Figure 2 bottom spectra), and similarly, the glycol-Pant and glycol-Ppant singly charged fragment ions showed the 57-Da increase expected from glycine addition (Figure 2, bottom). The glycolated Ppant-containing peptide eluted 30 s earlier than the Ppant-containing peptide, consistent with the addition of a charged chemical moiety (Figure S5, Supporting Information). By comparing the peak areas from extracted ion chromatograms of the doubly charged Ppant-containing and glycolated Ppant-containing peptides ( $m/z$  1134 vs  $m/z$  1163), we estimate that no more than 5% of the total holo-AlmF pool was glycolated when purified from *E. coli* expressing AlmE

(Figure S7, Supporting Information). Overexpression of AlmF alone yields relatively low protein levels (<1 mg/L of *E. coli*), suggesting that expression may be toxic in *E. coli*. Efficient glycolation may be impeded by other factors within *E. coli*, or conversely, another factor may be required for efficient glycolation of AlmF in *V. cholerae*. Because the *V. cholerae* biotype El Tor also contains lipid A modified with diglycine, we investigated whether holo-AlmF shuttles diglycine; however, our highly sensitive MS/MS protocols were unable to identify peaks associated with more than one glycine attached to AlmF (Figure S7, Supporting Information). As diglycine-modified lipid A is observed when isolated from *V. cholerae* biotype El Tor, it is likely that the terminal enzyme in the pathway, AlmG, can perform two rounds of glycolation. Dependent upon the El Tor strain, diglycine-modified lipid A can range from a minor to the most abundant lipid A species isolated.<sup>9</sup> Development of an assay for AlmG is currently underway in our laboratory. These results validate genetic and *in silico* predictions that AlmE activates glycine for transfer to the Ppant-containing carrier protein AlmF.

**AlmE Has Relaxed Substrate Selectivity for Amino Acids Other than Glycine.** To further explore the enzymology of AlmE, we developed a rapid *in vitro* assay that couples AlmE-catalyzed glycol-AMP formation with indirect detection of pyrophosphate, the other AlmE reaction product (see Figure 1). Pyrophosphatase was employed to convert pyrophosphate to phosphate, which was quantified using a spectrophotometric based malachite green assay.<sup>22</sup> *In vitro* AlmE assay conditions were optimized based on reports of previously characterized aminoacyl adenyltransferase/carrier protein ligases<sup>23–25</sup> (Supporting Information). Inclusion of purified holo-AlmF, compared to apo-AlmF, significantly stimulated activity as monitored by our pyrophosphatase-coupled assay (Figure S8, Supporting Information). Among a representative sampling of amino acids, glycine is the preferred substrate for adenylation; however, moderate activity (~25–30%) was observed when D-alanine was provided in AlmE reaction mixtures (Figure 3A). It should be noted that these assay conditions only monitor the ability to adenylate an amino acid and provide no information regarding subsequent ligation to holo-AlmF or other candidate acceptor substrates.

To more thoroughly monitor AlmE activity, we developed an alternative to the pyrophosphatase-coupled assay that could directly monitor the formation of  $^3\text{H}$ -aminoacyl-AlmF. Reaction products were TCA-precipitated, resuspended, then separated by SDS-PAGE and transferred to a nitrocellulose membrane for radioisotope detection. Formation of  $^3\text{H}$ -glycol-AlmF is indicated by the presence of the  $^3\text{H}$ -labeled protein band (Figure 3B), which is not observable when ATP or AlmE are omitted from assay mixtures (Figure 3B). We also tested other  $^3\text{H}$ -labeled amino acids, such as  $^3\text{H-L-alanine}$  and  $^3\text{H-D-alanine}$ . Consistent with our pyrophosphatase assays, AlmE activated and transferred  $^3\text{H-L-alanine}$  (<10%; compare Figure 3A to Figure 3B) but was unable to transfer  $^3\text{H-D-alanine}$  to holo-AlmF (Figure 3B). These data suggest that *V. cholerae* preferentially glycolates holo-AlmF, consistent with its mechanistic role in lipid A glycolation. Given the similarity of the active site to the D-alanine-specific enzyme DltA, it is not too surprising that AlmE showed some activity toward D-alanine. However, the activity seems to be restricted to adenylation, where subsequent ligation to carrier AlmF is not observed. As formation of an aminoacyl-adenylate is energetically costly, and AlmE exhibits modest activity toward D-alanine *in vitro*, it

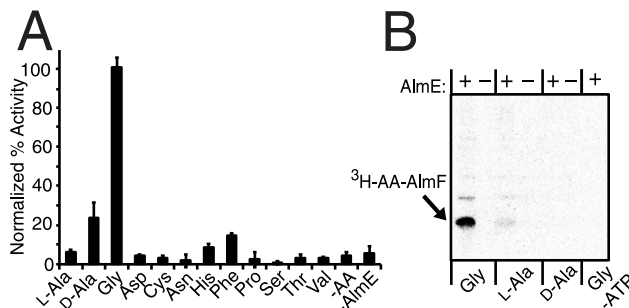


**Figure 3.** AlmE can efficiently adenylate glycine, and to a lesser extent, D-alanine. However, only glycine is efficiently transferred onto holo-AlmF under the described *in vitro* conditions. (A) Various amino acids (1 mM) were provided as substrates in pyrophosphatase-coupled AlmE (800 nM) assays. Control reactions are included where no amino acid was provided (−AA) or no enzyme was provided in the reaction (−AlmE). Percent activity was determined within the observed linear range of activity (2 h) and normalized to glycine-containing reactions (~35% activity overall). Activity measurements represent the % conversion of ATP (1 mM) supplied in the assay. Error bars denote the standard deviation of reactions as performed in triplicate. (B) Destabilizing urea-PAGE analysis of holo-AlmF, incubated with AlmE and the indicated  $^3\text{H}$ -amino acid *in vitro*, shows that AlmE can efficiently transfer activated glycine onto holo-AlmF, with trace activity observed when  $^3\text{H}$ -L-alanine is provided and no transferase activity when  $^3\text{H}$ -D-alanine is provided.

remains possible that AlmE can activate and transfer D-alanine to non-AlmF carrier substrates such as other carrier proteins or coenzyme A.

**Overall Structure of AlmE.** To better understand the features that govern substrate selectivity for glycine, we pursued the structural characterization of AlmE. No adenylation domains specific for this smallest amino acid have been deposited in the Protein Data Bank (PDB). AlmE formed narrow rod-shaped crystals with one monomer per asymmetric unit in space group  $P3_121$  (Table 1). Its structure was determined via molecular replacement to a resolution of 2.26 Å (Table 1). In addition to DltA enzymes, AlmE resembles the adenylation domains (A-domains) of nonribosomal peptide synthetases (NRPSs),<sup>26</sup> acyl- and aryl-CoA synthetases,<sup>27,28</sup> and firefly luciferases;<sup>29</sup> it comprises a large N-terminal body (50.6 kDa, residues 1–446), a smaller C-terminal lid (12.2 kDa, residues 450–556), and a very short hinge region (residues 447–449) linking the two domains (Figure 4A). On the basis of the studies of several related enzymes, AlmE crystallized in the thiolation conformation in which a channel for the 4'-phosphopanthetheinyl arm of AlmF is created through a ~140° rotation of the C-terminal lid relative to its position in the adenylation conformation.<sup>30</sup> Formation of the glycyl-adenylate intermediate was achieved by incubating AlmE with glycine, MgCl<sub>2</sub>, and ATP prior to crystallization (Figure 4B). No electron density is apparent for the His-tag, residues 1–14, and residues 25–29 that connect the N-terminus to the main body of the enzyme and residue 189, residues 533–536, or residues 551–556 of the C-terminus. Density for residues 15–24 is visible adjacent to the C-terminal lid of a symmetry mate, with residues 19–23 forming a short  $\beta$ -strand that runs antiparallel to the last  $\beta$ -strand (residues 523–527) of the neighboring lid.

The active site of AlmE is more similar to those of DltA enzymes (*Bacillus subtilis* DltA, PDB code 3E7W; *Bacillus cereus* DltA, PDB code 3DHV) than those of other adenylation domains whose coordinates have been deposited in the

**Table 1. Crystallographic Data and Refinement Statistics<sup>a</sup>**

data collection	
space group	$P3_121$
cell dimensions	
$a, b, c$ (Å)	116.2, 116.2, 99.6
$\alpha, \beta, \gamma$ (deg)	90.0, 90.0, 120.0
resolution (Å)	50–2.26 (2.30–2.26)
$R_{\text{merge}}$	0.107 (0.916)
$I/\sigma(I)$	16.6 (3.6)
no. of reflections	36632 (1800)
completeness (%)	99.9 (99.5)
redundancy	10.7 (10.0)
refinement	
resolution (Å)	50–2.26 (2.32–2.26)
$R_{\text{work}}/R_{\text{free}}$	0.166/0.193 (0.207/0.238)
no. of atoms	
protein	4214
ligand	27
water	157
average $B$ -factors (Å <sup>2</sup> )	
protein	33.9
ligand	28.6
water	33.5
RMS deviations	
bond lengths (Å)	0.008
bond angles (deg)	1.085
PDB code	4OXI

<sup>a</sup>Values in parentheses refer to the highest resolution shell.

PDB<sup>31,32</sup> (Figure 4C). DltA enzymes are D-alanyl carrier protein ligases that transfer D-alanine to lipoteichoic acids in the Gram-positive cell wall. The *B. subtilis* and *B. cereus* enzymes share 32% and 31% sequence identity with AlmE (Protein BLAST<sup>33</sup>), respectively, and their N-terminal bodies align with AlmE to 1.41 Å RMSD over 278 C<sub>α</sub> atoms and 1.59 Å RMSD over 289 C<sub>α</sub> atoms (PyMOL) (Figure S9, Supporting Information). Like AlmE, *B. subtilis* DltA was observed in the thiolation conformation, while *B. cereus* DltA was visualized in the adenylation conformation. *B. cereus* DltA, like AlmE, was crystallized bound to an aminoacyl-adenylate intermediate. With the AlmE structure, a Phyre2 model of AlmF, the *Streptomyces coelicolor* MatB structure (PDB code 3NYQ<sup>34</sup>), and the *E. coli* EntB-EntE complex structure (PDB code 3RG2<sup>35</sup>) as guides, the interaction between holo-AlmF and AlmE could be modeled (Figure S12, Supporting Information).

**Residues Contacting the Glycyl Moiety.** Several residues make favorable contacts general to all amino acyl groups, while others may play a greater role in enforcing glycine selectivity. The Lys452 amine forms a charged hydrogen bond with the glycyl carbonyl, while the carboxylate of Asp247 as well as the carbonyls of Gly341 and Ile347 (like Val301 of *B. cereus* DltA, Ile347 is in the disallowed region of the Ramachandran plot:  $\varphi, \psi = 75^\circ, -81^\circ$ ) make charged interactions with the positively charged glycyl amine. The residues of AlmE nearest the C<sub>α</sub> of the glycyl-adenylate, Leu248 (3.9 Å from C<sub>δ2</sub>) and Cys316 (3.4 Å from S<sub>γ</sub>), may select against amino acids larger than glycine by sterically clashing with their  $\alpha$ -substituents, Leu248 with the side chains of D-amino acids and Cys316 with those of L-amino acids. The conformation of Leu248 is determined through interactions with the side chains of the neighboring residues Phe246, Ser242, and Leu287. Ser242 and Leu287 are substituted with Ala192 and Thr240 in *B. cereus* DltA; their

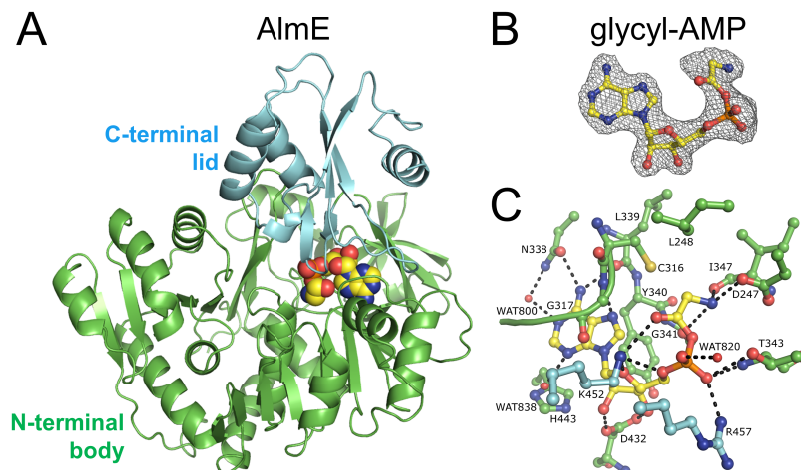


**Figure 4.** Crystal structure of AlmE with bound glycyl-AMP. (A) Cartoon representation of AlmE with glycyl-AMP (yellow spheres) bound between the N-terminal body (green) and C-terminal lid (cyan). AlmE is in the thioester-forming conformation in which the C-terminal lid has rotated  $\sim 140^\circ$  after forming the aminoacyl-adenylate intermediate. In this conformation, AlmE is prepared to transfer glycine from glycyl-AMP to the P<sub>pant</sub> arm of the carrier protein AlmF. (B)  $F_o - F_c$  electron density omit map of glycyl-AMP, contoured at 3 RMSD. (C) Binding mode of glycyl-AMP (yellow). The adenine ring is between His443, Ile365 (not pictured), and conserved Tyr340 on one side, and the Gly317-containing loop on the other. Residues contributed by the N-terminal body are green and those by the C-terminal lid are cyan. Hydrogen bonds are shown as dashed black lines. Some main chain atoms are hidden for clarity.

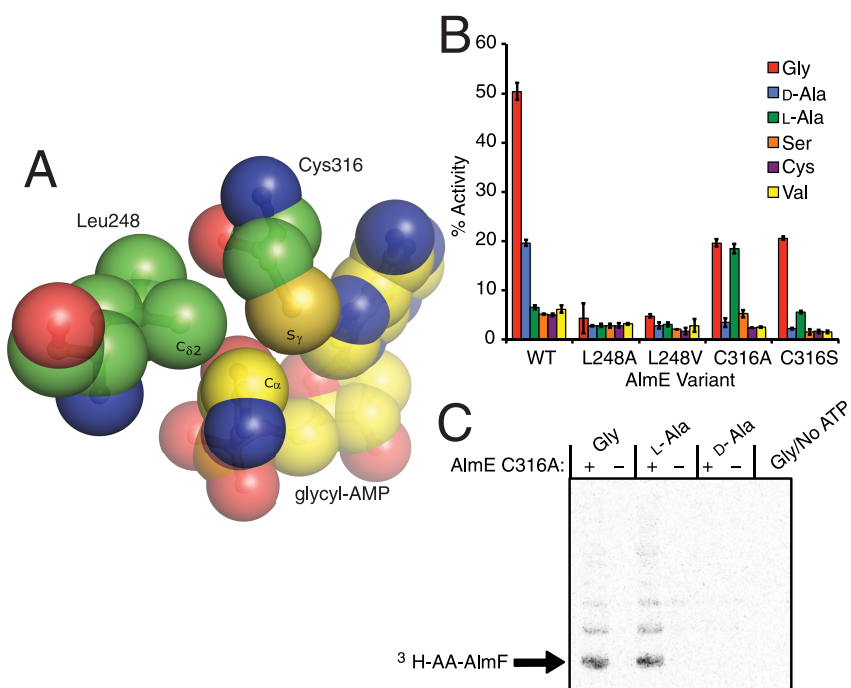


**Figure 5.** A rationally designed AlmE Cys316Ala variant shows relaxed specificity for L-alanine. (A) The side chains of Cys316 and Leu248, positioned above the C<sub>α</sub> of the glycyl-adenylate in the image, are hypothesized to exclude large amino acid chains via steric hindrance. Mutation of Cys316 and Leu248 to smaller amino acids might allow for relaxed specificity toward L- or D-amino acids, respectively. (B) All single-site AlmE variants display modest reduction in activity toward glycine; however, AlmE Cys316Ala shows relaxed specificity for the adenylation of L-alanine. AlmE variants (800 nM) were incubated with small amino acid substrates (1 mM) under standard pyrophosphatase-coupled assay conditions. Activities were measured in the linear range of wild-type AlmE for glycine. Activity measurements indicate the percent conversion of ATP (1 mM) supplied in the reaction, taken at 2.5 h. Error bars represent the standard deviation of reactions, measured in triplicate. (C) Destabilizing urea-PAGE analysis of holo-AlmF incubated with AlmE Cys316Ala and the indicated <sup>3</sup>H-amino acid *in vitro* shows that the Cys316Ala variant can efficiently transfer activated glycine or L-alanine to holo-AlmF.

smaller side chains position the C<sub>δ</sub> atoms of Leu198 (equivalent to Leu248 of DltA) farther from C<sub>α</sub> of the aminoacyl-adenylate than in AlmE, allowing room for the methyl group of D-alanine (Figure S9, Supporting Information). The helix containing Leu248 in AlmE is also straight, in contrast to the same helix in

DltA that creates space for the D-alanine methyl group through its bent geometry.<sup>31</sup> Structural evidence supports the hypothesis that Leu248 appears to contribute to stereoselectivity against D-amino acids, while Cys316 is positioned

to sterically select against L-amino acids with large C<sub>α</sub>-substituents.

**AlmE Variant Cys316Ala Can Efficiently Adenylate and Transfer L-Alanine to AlmF.** By comparing the active site architecture of AlmE with that of D-alanyl carrier protein ligase DltA, we predicted how glycine is selected over other small amino acids such as L- or D-alanine. On the basis of this analysis, as well as our observation that AlmE adenylates D-alanine and ligates L-alanine onto AlmF *in vitro* (Figure 3), we decided to investigate the specificity of AlmE through rational mutagenesis.

Single-residue variants of Leu248 and Cys316 were prepared with the hypothesis that less bulky side chains would relax the specificity of AlmE for D- or L-amino acids (Figure 5A). For example, such substitutions are present in the L-phenylalanine-specific PheA (PDB code 1AMU), L-leucine-specific SrfA-C (PDB code 2VQS), and L-valine-specific CytC1 (PDB code 3VNS) NRPS A-domains. Using site-directed mutagenesis, we prepared variants Cys316Ser, Cys316Ala, Leu248Val, and Leu248Ala and tested their specificity for glycine, D-alanine, L-alanine, L-serine, L-cysteine, and L-valine.

As expected, Leu248Val and Leu248Ala mutants did not improve AlmE specificity toward L-amino acids since Leu248 is positioned to sterically exclude side chains of D-amino acids (Figure 5B). However, these mutants also showed no activity toward D-alanine or glycine. This could indicate that Leu248 substitution significantly altered the geometry of the amino acid binding site, disrupting a number of the favorable binding interactions described above (Figure S9, Supporting Information). Our prediction that adequate space could be provided for an L-amino acid by mutating Cys316 appears valid. Replacement of the Cys316 sulfur atom with the relatively smaller oxygen atom, as in Cys316Ser, or removal of the thiol group, as in Cys316Ala, resulted in L-alanine adenylation. The Cys316Ser variant displayed reduced but modest activity for glycine and L-alanine relative to wild-type AlmE, while the Cys316Ala variant was equally able to adenylate glycine or L-alanine at levels below wild-type AlmE with glycine (Figure 5B). Furthermore, the AlmE Cys316Ala variant was equally able to form <sup>3</sup>H-glycyl- and <sup>3</sup>H-L-alanyl-AlmF, as determined by the destabilizing PAGE/radioisotopic assay described above (Figure 5C). As both Cys316Ser and Cys316Ala variants were less active for glycine adenylation than wild-type AlmE, it appears that substituting smaller side chains removes optimal packing interactions maintained between native AlmE and the C<sub>α</sub> of the glycyl group (Figure 5A). These results further indicate that the Cys316 thiol of wild-type AlmE sterically occludes all L-amino acids from the active site.

As the Cys316Ala mutant of AlmE was capable of adenylating and subsequently transferring glycine and L-alanine with nearly equal specificity, one could predict that L-alanyl-AlmF could serve as a substrate for AlmG for transfer onto lipid A. However, our MS analysis of *V. cholerae* lipid A expressing AlmE Cys316Ala did not show mass shifts consistent with L-alanine modification (Figure S10, Supporting Information). Nevertheless, this variant appears to be active, as we observed glycine-modified lipid A and restored polymyxin resistance in the polymyxin-sensitive *almE* mutant (Table S1, Supporting Information). On the basis of the absence of alanine-modified lipid A in the Cys316A mutant, coupled with the fact that low levels of L-alanyl-AlmF are generated by this variant in our *in vitro* assays, we propose that AlmG displays strict specificity for glycyl-AlmF.

The discovery of amino acid-modified *V. cholerae* lipid A revealed an interesting link between Gram-negative and Gram-positive cell surface modification systems, not only because the molecular pathways are remarkably similar but also because they confer a shared phenotypic outcome leading to polymyxin resistance. Here, we report the biochemical characterization of the initial steps of the AlmEFG lipid A glycation pathway required for polymyxin resistance in El Tor biotype *V. cholerae* O1, the causative agent of the ongoing cholera pandemic. By destabilizing urea-PAGE and mass spectrometry, we verified that AlmF is 4'-phosphopantetheinylated at Ser34 by Vc2457, a predicted 4'-phosphopantetheinyltransferase of the AcpS superfamily. With the same techniques, we were able to show that coexpression of AlmE in this strain results in the formation of glycyl-AlmF, consistent with our hypothesis that AlmF serves as a glycyl carrier protein (Figure 1). Furthermore, we carried out two different *in vitro* assays to corroborate how AlmE efficiently catalyzes the transfer of glycine to holo-AlmF. Taking into account that AlmG ultimately transfers glycine from glycyl-AlmF, we find that the overall pathway displays remarkable parallelism to the division of labor employed by nonribosomal peptide synthetases (Figure 1).

Our *in vitro* assays suggest that the substrate selectivity of AlmE is somewhat relaxed, adenylating D-alanine at a reduced level compared to that for glycine. In light of this finding, as well as the absence of structural data for an adenylate-forming enzyme with glycine specificity, we pursued the X-ray structure of AlmE. The enzyme crystallized in the thiolation conformation in which it is prepared to transfer a glycyl moiety to the 4'-phosphopantetheine of holo-AlmF. Electron density for the glycyl-adenylate intermediate was observed in the N-terminal body of AlmE. Given the similarity of the active site to the D-alanine-specific enzyme DltA, it was not too surprising that AlmE showed some activity toward D-alanine in the pyrophosphate release assay (Figure 3A and Figures S9 and S11, Supporting Information). However, we did not observe subsequent transfer of D-alanine onto AlmF (Figure 3B), and various attempts to substitute D-alanine for glycine in our crystallization conditions failed to produce AlmE crystals.

How D-alanine is transferred from carrier proteins to teichoic and lipoteichoic acid polymers in Gram-positive cell walls remains unknown but involves proteins DltB and DltD.<sup>36</sup> Similarly, characterization of AlmG (~30 kDa, membrane-associated, homologous to lysophospholipid acyltransferases, and lipid A lauroyl/myristoyl acyltransferases) will be necessary to clarify its role in the AlmEFG pathway.<sup>9</sup> The entire *almEFG* operon is conserved in the emerging marine pathogen *Vibrio nigrilurido*, although further study is required to verify whether this system can modify lipid A in this organism.<sup>37</sup> Glycine residues have been observed on the core-oligosaccharide of LPS in *Campylobacter jejuni*, *Haemophilus influenzae*, and *Shigella flexneri*.<sup>38–40</sup> It remains possible that these and other bacteria employ machinery similar to AlmEFG to decorate the carbohydrate and antigenic portion of LPS, not just the endotoxin portion of LPS as observed in *V. cholerae*.

Cationic antimicrobial peptides (CAMPs) are a therapy of last resort in the treatment of many bacterial infections. This report characterizes initial steps of a unique LPS modification strategy, employed by and necessary for CAMP resistance in *Vibrio cholerae*. As the AlmEFG system resembles Gram-positive cell-surface remodeling mechanisms, this study reveals how distantly related bacteria have evolved similar modes of antibiotic resistance: chemical modification of conserved

surface features. Recent reports suggest AlmEFG is important for host colonization by current pandemic *V. cholerae* El Tor. Because of the fitness advantage contributed by AlmEFG, as well as the nonfunctional operon encoded by previous pandemic classical *V. cholerae*, AlmEFG likely contributed to the emergence of El Tor as the current pandemic strain. As the role of glycine-modified LPS in host-pathogen dynamics and cholera disease progression becomes clearer, our structural evaluation of AlmE may provide the basis for rationally designed inhibitors of AlmE as a cholera therapeutic. Altogether, the structural and functional characterization of *V. cholerae* AlmE and AlmF presented here brings us closer to a comprehensive understanding of bacterial cell wall modification systems.

## METHODS

**Bacterial Growth.** Bacterial strains, plasmids, and oligonucleotides used in this study are listed in Tables S2 and S3 (Supporting Information). *V. cholerae* and *E. coli* were routinely grown at 37 °C on LB or LB agar unless otherwise indicated; 50 µg/mL kanamycin, 100 µg/mL ampicillin, and 10 µg/mL streptomycin were used as appropriate.

**Recombinant DNA Techniques.** Plasmids (Table S2, Supporting Information) were isolated using the QIAprep Spin Miniprep Kit (Qiagen). Custom primers were obtained from Integrated DNA Technologies (Table S3, Supporting Information). PCR reagents were purchased from Takara, New England Biolabs, or Stratagene, and PCR products were isolated using a QIAquick PCR Purification Kit (Qiagen). DNA fragments were isolated from 0.7% agarose gels using the QIAquick Gel Extraction Kit (Qiagen). All other DNA-modifying enzymes were purchased from New England Biolabs and used according to the manufacturer's protocols. When necessary, purity and yield of extracted DNA were monitored using a NanoDrop instrument (GE Healthcare). To create pQLink plasmids used for the coexpression of multiple genes, reagents purchased from Invitrogen were used for ligation-independent cloning (LIC) and as previously described.<sup>41</sup> All plasmids constructed in this study were transformed into a chemically competent *E. coli* XL-1 Blue storage strain before transformation into the strain used in experiments (Table S2, Supporting Information). Plasmid promoter and gene-insert sequences were verified by DNA sequencing at the ICMB Core Facility at the University of Texas at Austin.

**Cloning, Expression, and Purification of N-Terminal His<sub>6</sub>-AlmF or Coexpression Constructs.** Gene *almF* was PCR-amplified from El Tor biotype *V. cholerae* O1 strain N16961 genomic DNA (gDNA). *Bam*H I or *Hind*III restriction sites were engineered to flank the resultant PCR product using primers FpQlinkHVC1578 and RpQlinkHVC1578 (Table S3, Supporting Information). Both plasmid pQLinkH<sup>41</sup> and the PCR-amplified *almF* insert were restriction-digested, and plasmid DNA was treated with Antarctic phosphatase before ligation reactions were used to produce pQlinkHVC1578. The same cloning strategy was used to obtain pQlinkNVC0780, pQlinkNVC2457, and pQlinkNVC1579, where each gene was amplified using the corresponding primers by PCR with *V. cholerae* N16961 gDNA template (Table S3, Supporting Information). Coexpression constructs pQVC1578-Vc0780, pQVC1578-Vc2457, and pQVC1578-Vc2457-Vc1579 (Table S2, Supporting Information) were created using the standardized protocol as previously described.<sup>41</sup>

*Escherichia coli* BL21(DE3)pLysS cells containing the appropriate expression plasmid were grown in LB (1.5 L, 37 °C, 180 rpm shaking). Upon reaching an OD<sub>600</sub> of ~0.6, cultures were briefly chilled on ice to ~18 °C, and expression was induced by the addition of a sterile isopropyl β-D-1-thiogalactopyranoside (IPTG) solution (100 mM) to a final concentration of 1 mM. After 20 h (18 °C, 180 rpm), cells were pelleted, resuspended in ice-cold buffer A (500 mM NaCl, 50 mM 4-(2-Hydroxyethyl)piperazine-1-ethanesulfonic acid (HEPES) at pH 7.5, 10% (v/v) glycerol, 40 mM imidazole, and 1 mM dithiothreitol (DTT)) supplemented with 10 µM phenylmethylsulfonyl fluoride

(PMSF), and lysed via French press (20k psi). Lysate was clarified by centrifugation (4 °C, 20kg, 30 min), and the soluble portion was syringe-filtered (0.4 µm) before injection over an AKTA-compatible Ni-sepharose HiTrap FF column (GE Healthcare) pre-equilibrated with buffer A. The column was washed with buffer A (10 column volumes) before gradient elution over 30 column volumes to 100% buffer B (500 mM NaCl, 50 mM HEPES at pH 7.5, 10% (v/v) glycerol, 400 mM imidazole, and 1 mM DTT). One-milliliter fractions were collected where the peak Abs<sub>260</sub> fraction typically eluted between ~130–210 mM imidazole. Corresponding fractions with >80% AlmF, as determined by SDS-PAGE analysis (AlmF MW 8.9 kDa), were pooled and concentrated via filter centrifugation (Amicon Ultra, 3 kDa cutoff). To further purify AlmF, size-exclusion chromatography was performed using a Superdex S75 column (GE Healthcare) equilibrated with 1:5 dilution of buffer A (no imidazole). Concentrated Ni-sepharose-purified AlmF was diluted 1:5 in water before addition to the S75 column. Peak fractions were analyzed by SDS-PAGE, and fractions containing >95% AlmF were pooled and concentrated via filter centrifugation (Amicon Ultra, 3 kDa cutoff).

**Destabilizing Urea-PAGE of Purified AlmF Samples.** Urea-PAGE gels were manually cast using a mini-PROTEAN casting stand and frame (BioRad). Separating gel consisted of 13% polyacrylamide (19:1; Sigma-Aldrich), 2.5 M urea, 375 mM Tris at pH 9.5, 0.05% (w/v) ammonium persulfate (APS), and 0.05% (v/v) tetramethylethylenediamine (TEMED). Stacking gel consisted of 4% polyacrylamide (19:1; Sigma-Aldrich), 2.5 M urea, 125 mM Tris at pH 6.8, 0.05% (w/v) APS, and 0.1% (v/v) TEMED. Twenty micrograms of total protein was loaded per lane. Gels were run with prechilled running buffer (25 mM Tris base, 192 mM glycine, and 15% (w/v) urea, dissolved in ddH<sub>2</sub>O) in a 4 °C cold room for ~3–4 h at a constant 100 V. Visualization of protein bands was performed by Coomassie-staining for 24 h (45% (v/v) methanol, 10% (v/v) glacial acetic acid, 45% (v/v) ddH<sub>2</sub>O, and 3 g/L Coomassie R-250) and 24–48 h, due to the high % polyacrylamide, with destain solution (40% (v/v) ethanol, 10% (v/v) glacial acetic acid, and 50% (v/v) ddH<sub>2</sub>O). Gels were stored in ddH<sub>2</sub>O until photographically imaged.

**UVPD-MS Analysis of Tryptic Digested AlmF Samples.** Apo-AlmF, holo-AlmF (AlmF + Vc2457), and glycyl-AlmF (AlmF + Vc2457 + AlmE) samples were buffer-exchanged three times into 100 mM ammonium bicarbonate using 3 kDa molecular weight cutoff filters. Samples were then digested with trypsin (1:50 enzyme-to-substrate ratio) overnight and desalted. Peptides were evaporated to dryness and reconstituted in LC solvent A (98/2/0.1, water/acetonitrile/formic acid). For LC profiling, peptides were separated on a Dionex RSLCnano (ThermoDionex) using a gradient of 0–15% solvent B (100/0.1, acetonitrile/formic acid) over the course of 30 min and then up to 70% solvent B over 15 min. Flow rate was set to 750 nL/min through a 150 × 0.075 mm C18 analytical column packed in-house. The three most abundant multiply charged ions were selected for fragmentation using collision-induced dissociation (NCE 35) and subsequent detection in a Velos Pro dual linear ion trap mass spectrometer (ThermoFisher). Ultraviolet photodissociation spectra of the same peptides were acquired on an Orbitrap Elite mass spectrometer (ThermoFisher) after elution using the same gradient described previously on an Eksigent NanoLC Ultra (Eksigent) at a flow rate of 300 nL/min. UVPD was performed using 3 pulses of a 193 nm excimer laser (Coherent Excister XS) (at 3 mJ per pulse). The Orbitrap Elite mass spectrometer was modified and adapted for UVPD as described previously.<sup>42</sup> All spectra were manually interpreted.

**Cloning, Expression, and Purification of N-Terminal His<sub>6</sub>-AlmE or C316 and L248 Single Amino Acid Variants.** The *almE* gene was PCR-amplified from pVc1579<sup>9</sup> with primers F- and R-AlmE (Table S2, Supporting Information), cleaved with *Nhe*I and *Eco*RI, and ligated into pET28b (Novagen) to yield pETAlmE. C316S and L248V mutants were prepared by carrying out site-directed mutagenesis on pETAlmE (Table S2, Supporting Information) with the associated primers (Table S3, Supporting Information). C316S and L248V were further mutated to generate C316A and L248A with the associated primers (Tables S2 and S3, Supporting Information).

*Escherichia coli* BL21(DE3) cells containing the appropriate expression plasmid were grown in LB (1 L) with 50 mg/L kanamycin at 37 °C (180 rpm shaking). Upon reaching an OD<sub>600</sub> of ~0.5, cultures were briefly chilled on ice to ~18 °C, and expression was induced by the addition of a sterile IPTG solution (100 mM) to a final concentration of 1 mM. After 18 h (18 °C, 180 rpm), cells were pelleted, resuspended in ice-cold buffer A (500 mM NaCl, 50 mM HEPES at pH 7.5, 10% (v/v) glycerol, and 40 mM imidazole) supplemented with 10 μM PMSF, and lysed via French press (20k psi). Lysate was clarified by centrifugation (4 °C, 20kg, 30 min), and the soluble portion was syringe-filtered (0.4 μm) before injection over an AKTA-compatible Ni-sepharose column (GE Healthcare) pre-equilibrated with buffer A (no PMSF). The column was washed with buffer A (10 column volumes), before gradient elution over 30 column volumes to 100% buffer B (500 mM NaCl, 50 mM HEPES pH 7.5, 10% (v/v) glycerol, and 400 mM imidazole). One-milliliter fractions were collected where the peak Abs<sub>260</sub> fraction typically eluted between ~150–200 mM imidazole. Corresponding fractions with >95% AlmE, as determined by SDS-PAGE analysis (AlmE MW 63 kDa), were pooled and concentrated via filter centrifugation (Amicon Ultra, 3 kDa cutoff). For crystallization studies, Ni-sepharose-purified AlmE was further purified on a Superdex 200 gel filtration column (GE Healthcare) equilibrated with 150 mM NaCl, 10 mM HEPES at pH 7.5, and 10% (v/v) glycerol.

**In vitro AlmE Assays.** Glycine-containing AlmE/pyrophosphatase-coupled assay conditions are as follows: HEPES (50 mM, pH 7.5), KCl (100 mM), MgCl<sub>2</sub> (10 mM), ATP (1 mM), glycine (1 mM), yeast inorganic pyrophosphatase (Sigma, 0.5 U), purified holo-AlmF (8 μM), DTT (100 μM), and purified AlmE (800 nM) incubated at 25 °C for 2.5 or 3 h as indicated in the Results and Discussion section and/or figure legends. Percent activity corresponds to the percent conversion of [ATP] during AlmE catalyzed aminoacyl-AMP formation, where detected [phosphate]/2 equals [ATP] consumed. AlmF <sup>3</sup>H-aminoacetylation assays with AlmE were performed under identical reaction conditions as described above with omission of DTT and pyrophosphatase, inclusion of 0.3 μCi <sup>3</sup>H-amino acid, and were incubated for 18 h at 18 °C. AlmF in assay mixtures was concentrated by trichloroacetic acid (TCA) precipitation and resolved by SDS-PAGE. Resolved protein was transferred to a nitrocellulose membrane, which was exposed to a <sup>3</sup>H-sensitive screen for 5 days.

**Crystallization of AlmE.** Protein was concentrated to 10 mg mL<sup>-1</sup> in 10% (v/v) glycerol, 25 mM NaCl, and 10 mM HEPES at pH 7.5 and incubated with 10 mM glycine, 10 mM ATP, and 1 mM MgCl<sub>2</sub> for 10 min before preparing crystal trays. Narrow rod-shaped crystals grew in 50 mM MgCl<sub>2</sub> and 100 mM HEPES at pH 7.0 by sitting-drop vapor diffusion at 22 °C. Prior to flash freezing in liquid nitrogen, crystals were soaked for 10 min in cryosolution consisting of 20% (v/v) glycerol, 50 mM MgCl<sub>2</sub>, and 100 mM HEPES at pH 7.0. While crystals also grew in the absence of glycine and ATP, their quality and size were significantly diminished.

**X-ray Data Collection, Processing, Phasing, and Refinement.** Data were collected at 100 K at Advanced Photon Source Beamline 23-ID-D and processed in HKL2000<sup>43</sup> (Table 1). One crystal diffracted to 2.26 Å. Molecular replacement (MR) computations were performed in Phaser<sup>44</sup> with the N-terminal body of one monomer of PheA (PDB code 1AMU, residues 17–428) as a search model.<sup>26</sup> One AlmE monomer was found per asymmetric unit in space group P3<sub>1</sub>21. This solution was submitted to the ARP/wARP server for automated refinement<sup>45</sup> before iterative refinement was carried out in phenix.refine of the PHENIX software suite,<sup>46</sup> REFMAC5 of CCP4,<sup>44</sup> and Coot.<sup>47</sup> The structure factor amplitudes and atomic coordinates of AlmE were deposited in the RCSB Protein Data Bank under PDB code 4OXI.

**Polymyxin B and Polymyxin E Minimum Inhibitory Concentration Assay.** *V. cholerae* strains were grown overnight in LB media and then diluted 1:100 in fresh LB (1 mM IPTG, 100 μg/mL). Cells were grown to an OD<sub>600</sub> of ~0.6, diluted 1:100, and then applied to LB agar with a sterile cotton tip applicator. Quantitative minimum inhibitory concentration (MIC) values were determined

using Etest gradient polymyxin strips (AB Biodisk) after 24 h, using the manufacturer's guidelines.

**Matrix-Assisted Laser Desorption Ionization–Time-of-flight (MALDI-TOF) MS of Lipid A.** Lipid A was extracted, purified, and analyzed by MS as previously described.<sup>9,11</sup>

## ■ ASSOCIATED CONTENT

### S Supporting Information

MIC determination; information on the strains, plasmids, and primers utilized in this study; structural analysis of *V. cholerae* AlmF and related carrier protein domains; two-step purification of His<sub>6</sub>-AlmF; destabilizing urea-PAGE; reverse-phase HPLC chromatographic profiles; UVPD mass spectrum; extracted ion chromatograms; stereoview of the active sites of AlmE and *Bacillus cereus* DltA; MALDI-TOF mass spectrum; sequence alignment of a key specificity-encoding region of glycine-specific A-domains, AlmE, and DltAs; and model of the AlmE/AlmF complex. This material is available free of charge via the Internet at <http://pubs.acs.org>.

## ■ AUTHOR INFORMATION

### Corresponding Authors

\* (A.T.K.-C.) E-mail: adriankc@utexas.edu.

\* (M.S.T.) E-mail: strent@austin.utexas.edu.

### Author Contributions

<sup>†</sup>These authors contributed equally to this work.

### Notes

The authors declare no competing financial interest.

## ■ ACKNOWLEDGMENTS

Funding from National Institutes of Health (grants AI064184 & AI76322 to M.S.T., GM103655 to J.S.B., and GM106112 to A.T.K.), the Welch Foundation (F-1155 to J.S.B.), and the Army Research Office (grant W911NF-12-1-0390 to M.S.T.) is gratefully acknowledged. Instrumentation and assistance were provided by Macromolecular Crystallography Facility, financially supported by the College of Natural Sciences, the Office of the Executive Vice President and Provost, and the Institute for Cellular and Molecular Biology at UT Austin. Use of the Advanced Photon Source was supported by the U.S. DOE (Contract No. DE-AC02-06CH11357). We thank Thermo Fisher Scientific for help with the Orbitrap Elite mass spectrometer to allow UVPD.

## ■ REFERENCES

- (1) Li, J., Nation, R. L., Turnidge, J. D., Milne, R. W., Coulthard, K., Rayner, C. R., and Paterson, D. L. (2006) Colistin: the re-emerging antibiotic for multidrug-resistant Gram-negative bacterial infections. *Lancet Infect. Dis.* 6, 589–601.
- (2) Falagas, M. E., Rafailidis, P. I., Ioannidou, E., Alexiou, V. G., Matthaiou, D. K., Karageorgopoulos, D. E., Kapaskelis, A., Nikita, D., and Michalopoulos, A. (2010) Colistin therapy for microbiologically documented multidrug-resistant Gram-negative bacterial infections: a retrospective cohort study of 258 patients. *Int. J. Antimicrob. Agents* 35, 194–199.
- (3) Guilhelmelli, F., Vilela, N., Albuquerque, P., Derengowski, L. da S., Silva-Pereira, I., and Kyaw, C. M. (2013) Antibiotic development challenges: the various mechanisms of action of antimicrobial peptides and of bacterial resistance. *Front. Microbiol.* 4, 1–12.
- (4) Falagas, M. E., Rafailidis, P. I., and Matthaiou, D. K. (2010) Resistance to polymyxins: Mechanisms, frequency and treatment options. *Drug Resist. Updates* 13, 132–138.
- (5) Roy, H. (2009) Tuning the properties of the bacterial membrane with aminoacylated phosphatidylglycerol. *IUBMB Life* 61, 940–953.

- (6) Neuhaus, F. C., and Baddiley, J. (2003) A continuum of anionic charge: structures and functions of D-alanyl-teichoic acids in gram-positive bacteria. *Microbiol. Mol. Biol. Rev.* 67, 686–723.
- (7) Needham, B. D., and Trent, M. S. (2013) Fortifying the barrier: the impact of lipid A remodelling on bacterial pathogenesis. *Nat. Rev. Microbiol.* 11, 467–481.
- (8) Raetz, C. R. H., Reynolds, C. M., Trent, M. S., and Bishop, R. E. (2007) Lipid A modification systems in gram-negative bacteria. *Annu. Rev. Biochem.* 76, 295–329.
- (9) Hankins, J. V., Madsen, J. A., Giles, D. K., Brodbelt, J. S., and Trent, M. S. (2012) Amino acid addition to *Vibrio cholerae* LPS establishes a link between surface remodeling in gram-positive and gram-negative bacteria. *Proc. Natl. Acad. Sci. U.S.A.* 109, 8722–7.
- (10) Gangarosa, E. J., Bennett, J. V., and Boring, J. R. (1967) Differentiation between *vibrio cholerae* and *Vibrio cholerae* biotype El Tor by the polymyxin B disc test: comparative results with TCBS, Monsur's, Mueller-Hinton and nutrient agar media. *Bull. W. H. O.* 36, 987.
- (11) Hankins, J. V., Madsen, J. A., Giles, D. K., Childers, B. M., Klose, K. E., Brodbelt, J. S., and Trent, M. S. (2011) Elucidation of a novel *Vibrio cholerae* lipid A secondary hydroxy-acyltransferase and its role in innate immune recognition. *Mol. Microbiol.* 81, 1313–1329.
- (12) LaRocque, R. C., Harris, J. B., Dziejman, M., Li, X., Khan, A. I., Faruque, A. S. G., Faruque, S. M., Nair, G. B., Ryan, E. T., Qadri, F., Mekalanos, J. J., and Calderwood, S. B. (2005) Transcriptional profiling of *Vibrio cholerae* recovered directly from patient specimens during early and late stages of human infection. *Infect. Immun.* 73, 4488–4493.
- (13) Mandlik, A., Livny, J., Robins, W. P., Ritchie, J. M., Mekalanos, J., and Waldor, M. K. (2011) RNA-Seq-based monitoring of infection-linked changes in *Vibrio cholerae* gene expression. *Cell Host Microbe* 10, 165–174.
- (14) Crosby, J., and Crump, M. P. (2012) The structural role of the carrier protein – active controller or passive carrier. *Nat. Prod. Rep.* 29, 1111.
- (15) Beld, J., Sonnenschein, E. C., Vickery, C. R., Noel, J. P., and Burkart, M. D. (2014) The phosphopantetheinyl transferases: catalysis of a post-translational modification crucial for life. *Nat. Prod. Rep.* 31, 61.
- (16) Fischbach, M. A., and Walsh, C. T. (2009) Antibiotics for emerging pathogens. *Science* 325, 1089–1093.
- (17) Masoudi, A., Raetz, C. R. H., Zhou, P., and Pemble, C. W., IV (2013) Chasing acyl carrier protein through a catalytic cycle of lipid A production. *Nature* 505, 422–426.
- (18) Agarwal, V., Lin, S., Lukk, T., Nair, S. K., and Cronan, J. E. (2012) Structure of the enzyme-acyl carrier protein (ACP) substrate gatekeeper complex required for biotin synthesis. *Proc. Natl. Acad. Sci. U.S.A.* 109, 17406–17411.
- (19) Rock, C. O., Cronan, J. E., and Armitage, I. M. (1981) Molecular properties of acyl carrier protein derivatives. *J. Biol. Chem.* 256, 2669–2674.
- (20) Alberts, A. W., and Vagelos, P. R. (1966) Acyl carrier protein VIII. Studies of acyl carrier protein and coenzyme A in *Escherichia coli* pantothenate or B-alanine auxotrophs. *J. Biol. Chem.* 241, 5201–5204.
- (21) Kelly, W. L., Boyne, M. T., Yeh, E., Vosburg, D. A., Galonić, D. P., Kelleher, N. L., and Walsh, C. T. (2007) Characterization of the aminocarboxycyclopropane-forming enzyme CmaC. *Biochemistry (Moscow)* 46, 359–368.
- (22) Geladopoulos, T. P., Sotirodatis, T. G., and Evangelopoulos, A. E. (1991) A malachite green colorimetric assay for protein phosphatase activity. *Anal. Biochem.* 192, 112–116.
- (23) Osman, K. T., Du, L., He, Y., and Luo, Y. (2009) Crystal structure of *Bacillus cereus* d-alanyl carrier protein ligase (DltA) in complex with ATP. *J. Mol. Biol.* 388, 345–355.
- (24) Trauger, J. W., and Walsh, C. T. (2000) Heterologous expression in *Escherichia coli* of the first module of the nonribosomal peptide synthetase for chloroeremomycin, a vancomycin-type glycopeptide antibiotic. *Proc. Natl. Acad. Sci. U.S.A.* 97, 3112–3117.
- (25) McQuade, T. J., Shallop, A. D., Sheoran, A., DelProposto, J. E., Tsodikov, O. V., and Garneau-Tsodikova, S. (2009) A nonradioactive high-throughput assay for screening and characterization of adenylation domains for nonribosomal peptide combinatorial biosynthesis. *Anal. Biochem.* 386, 244–250.
- (26) Conti, E., Stachelhaus, T., Marahiel, M. A., and Brick, P. (1997) Structural basis for the activation of phenylalanine in the non-ribosomal biosynthesis of gramicidin S. *EMBO J.* 16, 4174–4183.
- (27) Jogl, G., and Tong, L. (2004) Crystal structure of yeast acetyl-coenzyme A synthetase in complex with AMP. *Biochemistry (Moscow)* 43, 1425–1431.
- (28) Gulick, A. M., Starai, V. J., Horswill, A. R., Homick, K. M., and Escalante-Semerena, J. C. (2003) The 1.75 Å crystal structure of acetyl-CoA synthetase bound to adenosine-5'-propylphosphate and coenzyme A. *Biochemistry (Moscow)* 42, 2866–2873.
- (29) Conti, E., Franks, N. P., and Brick, P. (1996) Crystal structure of firefly luciferase throws light on a superfamily of adenylate-forming enzymes. *Structure* 4, 287–298.
- (30) Wu, R., Reger, A. S., Lu, X., Gulick, A. M., and Dunaway-Mariano, D. (2009) The mechanism of domain alternation in the acyladenylate forming ligase superfamily member 4-chlorobenzoate: coenzyme A ligase. *Biochemistry (Moscow)* 48, 4115–4125.
- (31) Yonus, H., Neumann, P., Zimmermann, S., May, J. J., Marahiel, M. A., and Stubbs, M. T. (2008) Crystal structure of DltA: implications for the reaction mechanism of non-ribosomal peptide synthetase adenylation domains. *J. Biol. Chem.* 283, 32484–32491.
- (32) Du, L., He, Y., and Luo, Y. (2008) Crystal structure and enantiomer selection by d-alanyl carrier protein ligase DltA from *Bacillus cereus*. *Biochemistry (Moscow)* 47, 11473–11480.
- (33) Altschul, S. F., Madden, T. L., Schäffer, A. A., Zhang, J., Zhang, Z., Miller, W., and Lipman, D. J. (1997) Gapped BLAST and PSI-BLAST: a new generation of protein database search programs. *Nucleic Acids Res.* 25, 3389–3402.
- (34) Hughes, A. J., and Keatinge-Clay, A. (2011) Enzymatic extender unit generation for in vitro polyketide synthase reactions: structural and functional showcasing of *Streptomyces coelicolor* MatB. *Chem. Biol.* 18, 165–176.
- (35) Sundlov, J. A., Shi, C., Wilson, D. J., Aldrich, C. C., and Gulick, A. M. (2012) Structural and functional investigation of the intermolecular interaction between NRPS adenylation and carrier protein domains. *Chem. Biol.* 19, 188–198.
- (36) Reichmann, N. T., Cassona, C. P., and Grundling, A. (2013) Revised mechanism of D-alanine incorporation into cell wall polymers in Gram-positive bacteria. *Microbiology* 159, 1868–1877.
- (37) Goudenege, D., Labreuche, Y., Krin, E., Ansquer, D., Mangenot, S., Calteau, A., Médigue, C., Mazel, D., Polz, M. F., and Le Roux, F. (2013) Comparative genomics of pathogenic lineages of *Vibrio nigrilulchitudo* identifies virulence-associated traits. *ISME J.* 7, 1985–1996.
- (38) Dzieciatkowska, M., Brochu, D., van Belkum, A., Heikema, A. P., Yuki, N., Houliston, R. S., Richards, J. C., Gilbert, M., and Li, J. (2007) Mass spectrometric analysis of intact lipooligosaccharide: direct evidence for O-acetylated sialic acids and discovery of O-linked glycine expressed by *Campylobacter jejuni*. *Biochemistry (Moscow)* 46, 14704–14714.
- (39) Engskog, M. K. R., Deadman, M., Li, J., Hood, D. W., and Schweda, E. K. H. (2011) Detailed structural features of lipopolysaccharide glycoforms in nontypeable *Haemophilus influenzae* strain 2019. *Carbohydr. Res.* 346, 1241–1249.
- (40) Molinaro, A., Silipo, A., Castro, C. D., Sturiale, L., Nigro, G., Garozzo, D., Bernardini, M. L., Lanzetta, R., and Parrilli, M. (2007) Full structural characterization of *Shigella flexneri* M90T serotype 5 wild-type R-LPS and its galU mutant: glycine residue location in the inner core of the lipopolysaccharide. *Glycobiology* 18, 260–269.
- (41) Scheich, C., Kummel, D., Soumailakakis, D., Heinemann, U., and Bussow, K. (2007) Vectors for co-expression of an unrestricted number of proteins. *Nucleic Acids Res.* 35, e43–e43.
- (42) Shaw, J. B., Li, W., Holden, D. D., Zhang, Y., Griep-Raming, J., Fellers, R. T., Early, B. P., Thomas, P. M., Kelleher, N. L., and

Brodbelt, J. S. (2013) Complete protein characterization using top-down mass spectrometry and ultraviolet photodissociation. *J. Am. Chem. Soc.* 135, 12646–12651.

(43) Otwinowski, Z., and Minor, W. (1997) Processing of X-ray diffraction data collected in oscillation mode. *Methods Enzymol.* 276, 307–326.

(44) Winn, M. D., Ballard, C. C., Cowtan, K. D., Dodson, E. J., Emsley, P., Evans, P. R., Keegan, R. M., Krissinel, E. B., Leslie, A. G. W., McCoy, A., McNicholas, S. J., Murshudov, G. N., Pannu, N. S., Potterton, E. A., Powell, H. R., Read, R. J., Vagin, A., and Wilson, K. S. (2011) Overview of the CCP 4 suite and current developments. *Acta Crystallogr., Sect. D* 67, 235–242.

(45) Langer, G., Cohen, S. X., Lamzin, V. S., and Perrakis, A. (2008) Automated macromolecular model building for X-ray crystallography using ARP/wARP version 7. *Nat. Protoc.* 3, 1171–1179.

(46) Adams, P. D., Afonine, P. V., Bunkóczki, G., Chen, V. B., Davis, I. W., Echols, N., Headd, J. J., Hung, L.-W., Kapral, G. J., Gross-Kunstleve, R. W., McCoy, A. J., Moriarty, N. W., Oeffner, R., Read, R. J., Richardson, D. C., Richardson, J. S., Terwilliger, T. C., and Zwart, P. H. (2010) PHENIX: a comprehensive Python-based system for macromolecular structure solution. *Acta Crystallogr., Sect. D* 66, 213–221.

(47) Emsley, P., and Cowtan, K. (2004) Coot: model-building tools for molecular graphics. *Acta Crystallogr., Sect. D* 60, 2126–2132.